Robust approach to directly measuring water-leaving radiance in the field

ZhongPing Lee,[1,*] Nima Pahlevan,[1] Yu-Hwan Ahn,[2] Steven Greb,[3] and David O'Donnell[4]

[1]Department of Environmental, Earth and Ocean Sciences, University of Massachusetts Boston, 100 Morrissey Blvd., Boston, Massachusetts 02125, USA

[2]Korea Institute of Ocean Science & Technology, P.O. Box 29, Ansan 425-600, South Korea

[3]Wisconsin Department of Natural Resources, 101 South Webster Street, Madison, Wisconsin 53703, USA

[4]Upstate Freshwater Institute, P.O. Box 506, Syracuse, New York 13214, USA

*Corresponding author: zhongping.lee@umb.edu

Received 5 December 2012; revised 3 February 2013; accepted 6 February 2013; posted 12 February 2013 (Doc. ID 181179); published 7 March 2013

It has been a long-standing goal to precisely measure water-leaving radiance (L_w, or its equivalent property, remote-sensing reflectance) in the field, but reaching this goal is quite a challenge. This is because conventional approaches do not provide a direct measurement of L_w, but rather measure various related components and subsequently derive this core property from these components. Due to many uncontrollable factors in the measurement procedure and imprecise post-measurement processing routines, the resulting L_w is inherently associated with various levels of uncertainties. Here we present a methodology called the skylight-blocked approach (SBA) to measure L_w directly in the field, along with results obtained recently in the Laurentian Great Lakes. These results indicate that SBA can measure L_w in high precision. In particular, there is no limitation of water types for the deployment of SBA, and the requirement of post-measurement processing is minimum; thus high-quality L_w for a wide range of aquatic environments can be acquired.

OCIS codes: 010.0010, 010.4450, 120.0120, 120.0280.

1. Introduction

Spectral water-leaving radiance (L_w, μW/cm^2/nm/sr), or its equivalent, spectral remote-sensing reflectance (R_{rs}, sr^{-1}, which is defined as the ratio of L_w to downwelling irradiance just above the surface ($E_d(0^+)$, μW/cm^2/nm), is a core property for optical oceanography. Subsurface properties, such as inherent optical properties or chlorophyll concentration, as well as bottom properties of optically shallow waters, are all derived by inverting the R_{rs} spectrum [1,2]. Separately, properties of L_w are key in validating those that are derived from airborne or spaceborne sensors and systems [3–8]. Furthermore, L_w values within the red/near-infrared (800–1000 nm) and shortwave infrared (1000–2500 nm) bands, progressively assumed to be zero for different loads of suspended materials, are used in the atmospheric correction process [9–12]. Because of such critical importance, measurement of spectral L_w in the field has been carried out for more than five decades, and generally three approaches have been developed and implemented [13–15]. Table 1 summarizes the advantages and drawbacks of these schemes, while the following provides a brief description of each approach.

Scheme 1 (S1):
Measure all relevant properties from an above-surface platform, and then calculate L_w by removing surface-reflected light.
Scheme 2 (S2):
Measure the vertical profiles of upwelling radiance ($L_u(z)$) within the water column, mathematically

1559-128X/13/081693-09$15.00/0

Table 1. Summary of the Conventional Schemes in Obtaining L_w in the Field

	Advantages	Limitations
S1: Above-surface method	Can be used in any environment; no self-shading	Measures L_T in the air, not L_w; includes surface-reflected light, requires sophisticated postprocessing to correct surface-reflected light.
S2: In-water profiling method	Avoids surface-reflected light	Measures L_u, not L_w; slight self-shading; requires sophisticated postprocessing to derive L_w; difficult to extrapolate upwelling radiance at a depth to surface for waters that are stratified or with a shallow bottom (e.g., kelp fields)
S3: Surface floating method	Avoids surface-reflected light	Measures L_u, not L_w; slight self-shading; requires careful postprocessing to L_w

propagate these measurements upward toward the sea surface, and then across the surface to get L_w.
Scheme 3 (S3):
Measure $L_u(z)$ a few centimeters below the surface, and then mathematically propagate $L_u(z)$ across the surface to obtain L_w.

All of these schemes are easily implementable in the field, but they never measure L_w directly, which leads to nonnegligible uncertainties associated with L_w produced by these schemes [13,16]. As discussed in numerous studies, when estimating L_w using method S1, it is quite a challenge to accurately remove the surface-reflected light when the sea surface is roughened by waves, where the reflected light includes both sky and sun glint [13,17,18]. The effective reflectance of the sea surface is highly wavelength- and data-collection-dependent [13,19,20]. The S2 method involves delicate data processing to derive the appropriate attenuation coefficient in order to propagate $L_u(z)$ to the surface [21]. More importantly, for highly turbid waters or vertically stratified waters, it is very difficult to achieve an accurate estimation of the attenuation coefficient for this propagation [22]. For S3, because the measurement is $L_u(z)$, it requires propagating $L_u(z)$ (where z is typically 10–50 cm) to $L_u(0-)$. Further, for both S2 and S3, $L_u(0-)$ has to be subjectively propagated to L_w by assuming values about the refractive index of water and the cross-surface reflectance [23]. Consequently, various levels of uncertainties are associated with the *calculated* L_w even if each component is measured perfectly. In this study, we demonstrate a hybrid approach that measures L_w directly, and show that the approach can achieve high-precision measurement of L_w in the field.

2. Approach to Directly Measuring L_w

To maximize the advantages while avoiding the drawbacks associated with the traditional measurement schemes (S1–S3), a hybrid scheme was first utilized by Ahn [24]. This method, which collects upwelling radiance from a position above the sea surface while effectively blocking surface-reflected light with an apparatus, measures L_w directly in the field. The concept and strategy of this skylight-blocked approach (SBA) is presented in Fig. 1. The whole system includes a radiometer and a black cone (see Fig. 2, left panel). The cone is attached to the sensor with its open end inserted just below the surface, while the radiometer maintains a position in the air (see Fig. 2, right panel); thus the measured property by the radiometer is L_w. In such a setup, the below-surface $L_u(0-)$ propagates to L_w naturally and surface-reflected light is blocked mechanically, thus removing two post-measurement processing steps that introduce uncertainties in the traditional schemes.

The cone used in our system, which was custom manufactured to fit the HyperOCR radiometer (Satlantic, Inc.), has a diameter 9.8 cm and a height 10.1 cm, optimized not to interfere with the field of view of HyperOCR (11.5°) while minimizing the effect of self-shading [25]. Integrated with the Satlantic HyperPro Profiler, the system floats on the sea surface and can be deployed well away from the boat to avoid its interference to the light field. This SBA is especially useful for vertically stratified waters or coastal environments including kelp beds shallow bottoms, where it is difficult to obtain a viable profile of $L_u(z)$ for the propagation. More importantly, because this SBA avoids the complicated postprocessing in deriving L_w, significantly less uncertainty is anticipated in the field-measured L_w spectrum. The second-order effects from slight self-shading can be corrected (in preparation), as shown in Gordon and Ding [25] and Leathers *et al.* [26].

3. Field Measurements

Recently, we deployed a HyperOCR (350–800 nm, ~3 nm resolution) via the SBA to measure L_w in the zenith direction in Lake Michigan and Green Bay

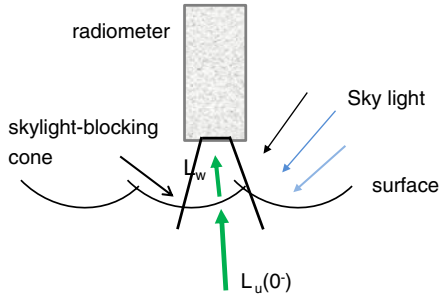

Fig. 1. (Color online) Schematic draw to show the concept of measuring L_w directly in the field. The cone is integrated with a radiometer to block surface-reflected light, with its open end inserted just below (~5 cm) the surface when measuring L_w.

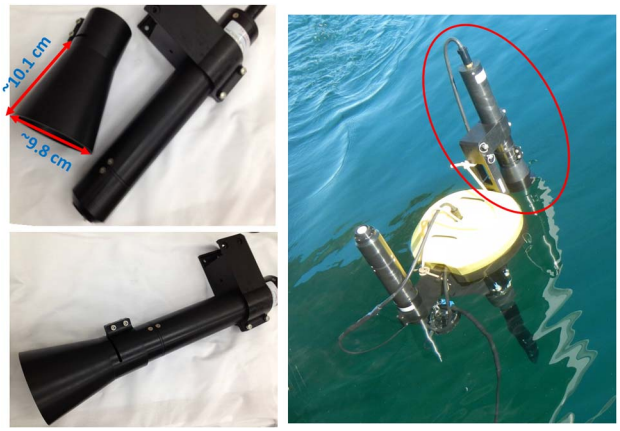

Fig. 2. (Color online) (Left) Cone and radiometer. (Right) The system is deployed in the field.

(June 25–28, 2012). Concurrent with the L_w measurements, another HyperOCR irradiance radiometer was used to measure downwelling irradiance just above the surface ($E_d(0+)$). The right panel in Fig. 2 shows the two radiometers, with the one in the red circle for the measurements of L_w via SBA. A total of 19 stations were surveyed (see Fig. 3 for locations), with sea surface ranging from calm (<1′ wave height) to rough (~2′–3′ wave height) conditions. Sun angle varied in a range of ~20°–50° from zenith, and one-third of the stations had a sky covered with scatter clouds. The stations covered waters with a wide range of variability in biogeochemical properties, as indicated by the spectral R_{rs} (see Fig. 4), which were derived from L_w and $E_d(0+)$ spectra measured simultaneously and averaged for each station. The coefficient of variation (CV) of all measured R_{rs} ranges from ~50% (at 530 nm) to >80% (for UV and red-infrared wavelengths).

Along with the measurements via SBA, concurrent measurements of $L_u(z)$ were made following the profiling scheme (S2). For this deployment (two stations were omitted, so S2 covered 17 stations), radiometric measurements were made with a HyperPro II profiling system (Satlantic, Inc.), where one HyperOCR measures $L_u(z)$, another HyperOCR

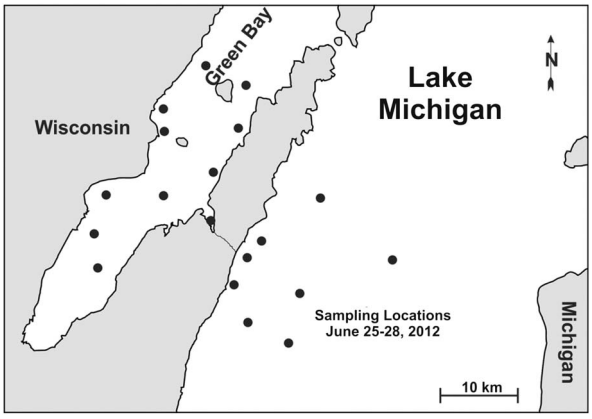

Fig. 3. Stations surveyed in Lake Michigan and Green Bay, June 2012.

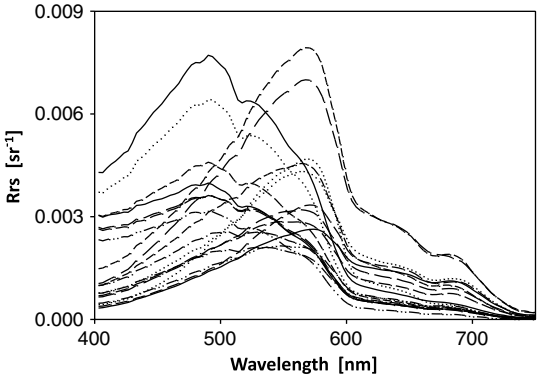

Fig. 4. R_{rs} spectra of the 19 stations measured via SBA.

measures $E_d(z)$, and a third HyperOCR located on deck measures solar irradiance above the water surface ($E_d(0+)$). The profiler freefalls through the water column with a descending rate at ~25 cm/s, and three back-to-back (triplicates) profiles were measured at each station.

Both systems were tethered from a small boat at least ~20 m away, and the two systems were ~20 m apart.

Also measured for each station were the total absorption and beam attenuation coefficients in the upper water column with the ac-s system (Wetlabs, Inc.), which was calibrated with DI-water and lowered into water by the side of the operating boat. The total absorption coefficient at 440 nm spanned a range of 0.13–0.7 m^{-1}, while the beam attenuation coefficient at 660 nm ranged 0.26–0.9 m^{-1}. The vertical profiles of these data did not show significant stratification of optical properties in the upper water column (20 m) during this experiment.

4. Data Processing

A. L_w Measurements via SBA

In addition to applying common data-processing procedures (e.g., application of calibration coefficient, tilt-angle based filtering), the L_w data collected via SBA went through two extra quality-control processes.

First, there are two situations in which the data collected via SBA could be contaminated, and both may happen when the sea surface is under rough conditions. One situation is where the radiometer (along with the cone) is submerged below the sea surface; then the collected data represents upwelling radiance at a depth a few centimeters below the surface ($L_u(z)$), which may approximate the upwelling radiance just below the surface ($L_u(0-)$). The other situation is where the entire cone swings above the sea surface; then the data collected represents upwelling radiance above the surface (L_T). Data collected under these two conditions do not represent L_w and should be removed.

In this step of data processing, which is aimed at removing the contaminated data mentioned above, the higher values in each set of L_w measurement were identified and filtered out. This is achieved

by calculating the median (μ) and standard deviation (σ) of L_w for wavelengths (λ) longer than 750 nm of each L_w set, and the spectrum with a spectrally averaged value for λ between 750 and 800 nm greater than ($\mu + 3\sigma$) was considered contaminated and removed. This is based on the following general relationship:

$$L_T(\lambda) = L_w(\lambda) + L_g(\lambda) \quad (1)$$

and

$$L_w(\lambda) = \frac{t}{n^2} L_u(\lambda, 0-) \quad (2)$$

with L_g the surface-reflected light (including glints from both sky and solar light). t is the transmittance, n the refractive index of seawater, and $t/n^2 \approx 0.54$ [23,27].

From Eqs. (1) and (2), we have $L_w < L_u(0-)$ and $L_w < L_T$. Therefore, the high values in each set of L_w measurement represent $L_u(0-)$ or L_T. Also, because L_w is generally very small in the longer wavelengths for most aquatic environments [28], the use of information of wavelengths longer than 750 nm makes it easier to identify surface-reflected light. Figure 5 shows an example where outliers [the red (top) line] are detected and removed from further processing. For this station, there were 63 valid L_w spectra after applying tilt filtering (Satlantic, Inc.), one spectrum was further removed based on the above procedure, and the mean of the remaining 62 spectra was calculated to represent the water-leaving radiance of this station. Also showing in Fig. 5 is the spectrum of CV of this station (calculated as the ratio of standard deviation to the mean at each spectra band) from the remaining 62 L_w spectra. Although we kept >98% of the original data, the CV is generally within 10% for the 400–700 nm range (more discussions regarding CV are presented in Section 5.B). In our datasets collected during June 2012, on average less than 3% of the measured spectrum at each station was discarded following the above process, indicating that nonaggressive filtering of the data was processed for results in this study.

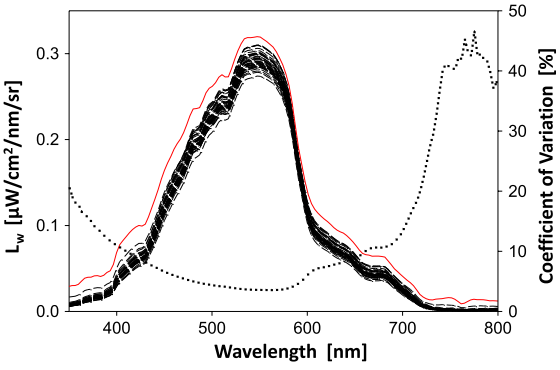

Fig. 5. (Color online) Example showing L_w spectra collected by HyperOCR through SBA. The red (top) line (1 out of 63 spectra) was considered as an outlier and excluded for further processing and calculation. Also shown is the spectrum of CV (right Y axis) of the remaining 62 L_w spectra.

Second, as a first-order self-shading correction, the formula developed by Gordon and Ding [25] was used to account for the instrument shading effects associated with SBA. Basically, self-shading is modeled as a function of absorption coefficient and sun-zenith angle [25], and the concurrent measurement of total spectral absorption by the ac-s system (covers 405–720 nm) was used for this correction. While the instrument configuration in our study was not identical to that modeled by Gordon and Ding [25], it is expected that the analytical approach accounts for self-shading impacts at least to the first order.

B. L_w Collection from Vertical Profiles

Processing of measurements from the profiler followed the protocol and software (ProSoft version 7.7.16_6, the most recently generally available release) provided by Satlantic, Inc. Basically, for each profile measurement, least-square regression was carried out between the logarithm-transferred $L_u(z)$ and z (generally within 20 m depth) for measurements in the upper water column [13,21], resulting in an intercept and slope, with the former providing the logarithm of $L_u(0-)$ and the latter representing the diffuse attenuation coefficient of $L_u(z)$ (K_{Lu}). The mean and standard deviation of $L_u(0-)$ were calculated from the three back-to-back profiles for each station. We used 0.5 m bins with 0.1 m depth interpolation for this processing. We also explored using a smaller bin size, but found no systematic change in the resulting $L_u(0-)$ and its CV. The water-leaving radiance L_w is then calculated using Eq. (2). No self-shading correction was applied to profiling data since there are no known methods yet to accurately correct the vertically varying self-shading effects. This is also due to the fact that the biggest impact of applying this shading correction will be on the derived value of $L_u(0-)$ of each profile, not on the CV of $L_u(0-)$ when analyzing the three profiles. And the focus of this study is the precision in the measurement of L_w, which is measured by its CV; thus omitting the self-shading correction in the processing of $L_u(z)$ is appropriate here.

5. Results

A. Comparison of Overall L_w Spectrum

As an example, Fig. 6 shows spectral L_w obtained from the SBA and the profiling (S2) scheme. The comparison is limited to wavelengths in the range of 405–720 nm, as that is the range where self-shading correction was applied to SBA-measured L_w. Apparently, both schemes produced quite consistent L_w, although the L_w from SBA is roughly ~11% lower than that from S2 for this station. For all 17 coincidental stations, on average, the mean L_w of each station obtained from the two schemes is very consistent [see Fig. 7(a)]. The coefficient of determination (R^2) is

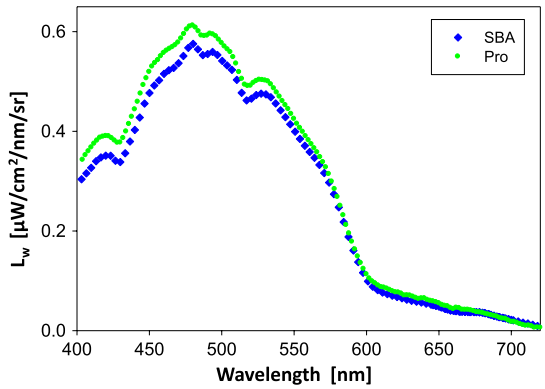

Fig. 6. (Color online) Example to compare the L_w spectra measured via SBA and profiling.

0.98, with a slope of 1.005 (L_w from S2 is slightly larger) and close to 0 interception.

To further evaluate the two L_w datasets, the percentage difference (PD) between the SBA-measured L_w (SBAL_w) and the profile-measured L_w (ProL_w) for each band of each station is calculated as

$$\mathrm{PD}(\lambda) = \frac{2(\mathrm{SBA}L_w(\lambda) - \mathrm{Pro}L_w(\lambda))}{(\mathrm{SBA}L_w(\lambda) + \mathrm{Pro}L_w(\lambda))}. \quad (3)$$

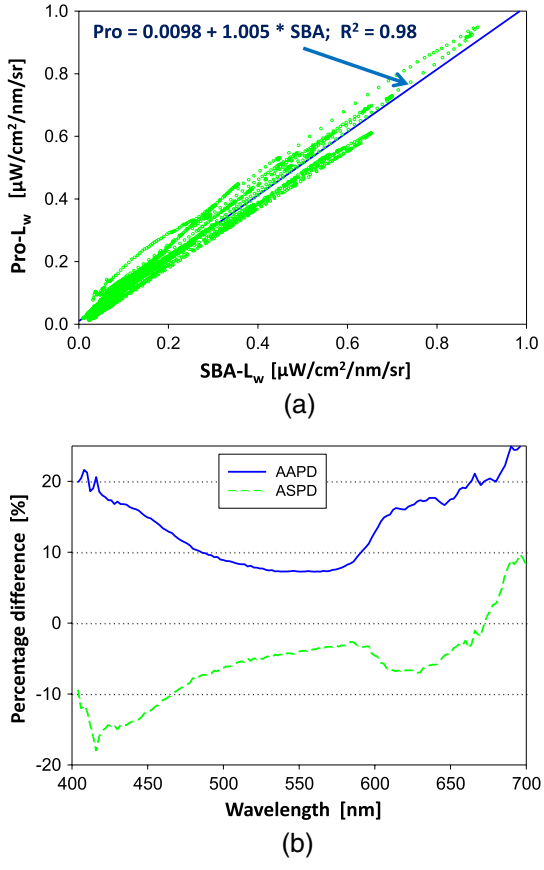

Fig. 7. (Color online) (a) Statistic relationship between SBA-measured and pro-measured L_w, for wavelength in the range of 405–720 nm. (b) Percentage difference (PD) between SBA-measured (SBAL_w) and pro-measured (ProL_w) L_w. PD is defined as $2(\mathrm{SBA}L_w - \mathrm{Pro}L_w)/(\mathrm{SBA}L_w + \mathrm{Pro}L_w)$. AAPD stands for the average of the absolute value of PD, while ASPD stands for the average of the signed PD.

Figure 7(b) presents the spectra of the average of the absolute value of PD (AAPD), and of the average of the signed value of PD (ASPD), respectively, of the 17 stations. Apparently, for this experiment, larger difference or uncertainty (~20%) exists at both shorter (~400 nm) and longer (~700 nm) wavelengths, and SBAL_w is generally lower than ProL_w except at the longer wavelengths. For the transparency window where L_w values are much higher than those at the two spectral ends (see Fig. 5, for example), however, the L_w values from the two systems are quite close (<10% difference), echoing the difficultly in obtaining confident measurement of L_w in the field when its value is small [18,29].

It is difficult to determine which system provided a more accurate measurement of L_w during this experiment, because the L_w values from both systems contain some levels of errors. First, radiometric calibration of the two radiometers was not completed simultaneously; some drifting in the calibration coefficient of either sensor or both could contribute to the difference. Second, the two systems had different self-shading effects, where one happens near the sea surface, while the profiling system experiences shading in the entire profiling process and no shading correction was applied to the $L_u(z)$ data. And third, there are always uncertainties when propagating $L_u(z)$ to L_w. Nevertheless, the quite consistent L_w values shown in Fig. 7(a) suggest that, on average, L_w obtained from both systems is valid.

B. Comparison of L_w Precision

Although it is useful and necessary to check the consistency of L_w measured from different systems/schemes [13,16,30], it is equally or more important to know how precise each measured L_w spectrum is. To obtain an objective characterization of this precision (or stability) of L_w measured via SBA, we calculated the CV spectrum of each station as shown in Fig. 8, and then the average and standard deviation

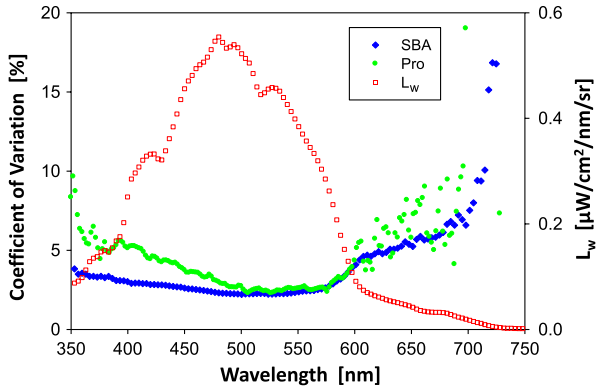

Fig. 8. (Color online) Example to compare the spectral CV of L_w measured via SBA and profiling. Also shown is the L_w spectrum (right Y axis) of this station.

of these CV spectra. As a preliminary contrast and comparison, the same calculations were carried out on the data obtained via the profiling system (S2). As an example, Fig. 8 compares the CV spectra resulting from SBA and from S2 to the L_w spectra presented in Fig. 6. For this station, CV from the SBA measurement is 3%–5% for wavelengths in the range of 350–600 nm (or $L_w > 0.06$ μw/cm^2/nm/sr), while the CV from the S2 measurement is 3%–10% for the same spectral range. For the 600–750 nm range, CV of L_w from S2 is generally 30% higher than that from SBA. This is partially because in the longer wavelengths the light attenuates significantly with the increase of depth due to the high absorption coefficient of water molecules; thus it is difficult to maintain high-precision measurement of such low light. Although higher CV is generally expected when L_w is approaching zero, this example demonstrates that for the same range of L_w, CV from the SBA is systematically smaller than that from the profiling.

To further highlight the significantly better precision of SBA-measured L_w, Figs. 9(a) and 9(b) show the mean spectral CV (along with its standard deviation) of the 17 coincidental stations from the two schemes, respectively. For L_w from SBA, the averaged CV is below 5% for wavelengths in the range of 400–650 nm [Fig. 9(a)]; however it is 10%–40% when L_w is obtained from S2 [Fig. 9(b)]. For the shorter (350–400 nm) and longer (650–750 nm) wavelengths where L_w values are quite low for these measurements, the averaged CV (350–400 nm) remains below 10% when L_w was measured via SBA, but it is greater than 30% when L_w was derived from profiles, and the CV (650–750 nm) of L_w from profiles is generally twice the CV (650–750 nm) when L_w was measured via SBA. Furthermore, for L_w measured via SBA, most (greater than 67%) of its CV values are within 5%, but only ~30% of its CV values are within 5% when L_w was determined from profiles (see Fig. 10). All of these results indicate that SBA indeed achieved high-precision measurement of L_w in the 350–700 nm range, at least for waters and sea states in this experiment. Note that because of the repetitive measurements at each station, not only could the average value of L_w be derived and reported, but also could the associated uncertainty (e.g., Fig. 8) of the measured L_w—and the latter is an important measure of the quality of reported L_w.

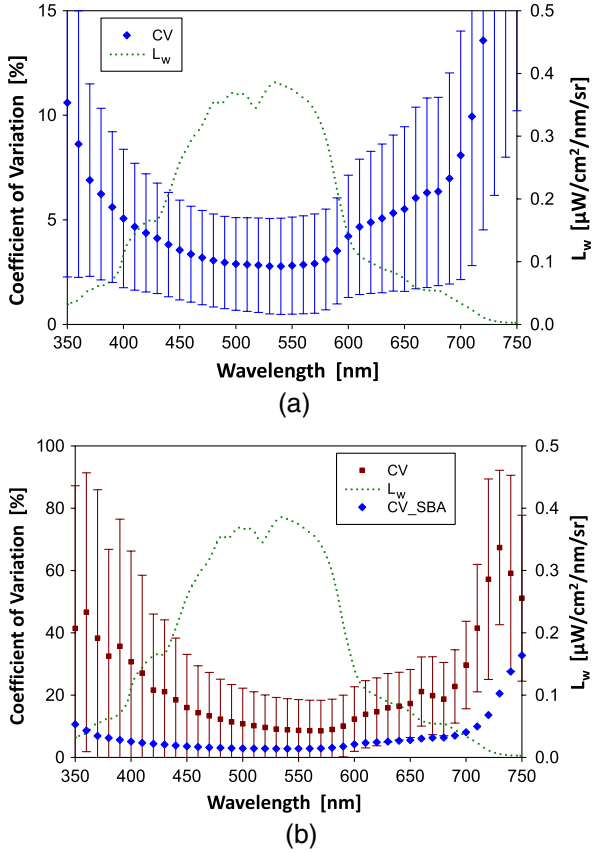

Fig. 9. (Color online) (a) Averaged spectrum of CV of all stations. Dotted green curve provides crude information of the L_w (SBA measured) encountered, as there is a wide range of variation. (b) Averaged CV spectrum of L_w measured from profiles. Also included (blue dots) is the mean CV spectrum from SBA for easier comparison.

This high-precision measurement of L_w via SBA is important in the determination of R_{rs}, as it is not a must to have radiometrically accurate L_w for its derivation. When a calibrated reference panel is used in the process [14,30,31], measurements of L_w in relative units instead of absolute radiometric units is sufficiently reliable for the determination of R_{rs}. In such a setup, the precision rather than the accuracy of L_w measurement is more important, and the accuracy of R_{rs} will depend on the accuracy of the reference panel used to measure $E_d(0+)$ [14,31,32] when all other aspects of measurements are well handled.

6. Discussion and Future Perspective

Spectral water-leaving radiance (L_w), or spectral remote-sensing reflectance (R_{rs}), plays a critical role in ocean optics and ocean-color remote sensing. L_w (or R_{rs}) is the property required for validation of ocean-color satellite systems (from sensor calibration to atmospheric correction), the input for the retrieval

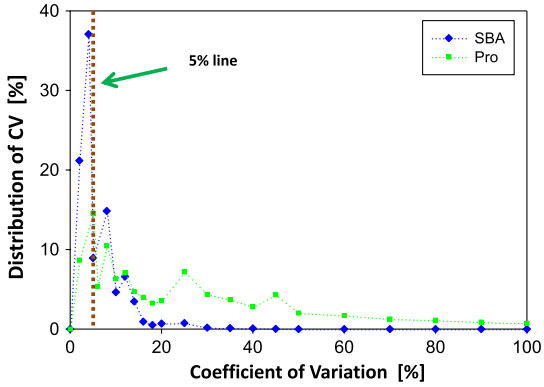

Fig. 10. (Color online) Distribution of the CV of L_w measured via SBA and profiling, respectively. Wavelength range is 350–720 nm.

of subsurface properties and constituents, and a property to evaluate the closure of the relationship between inherent and apparent optical properties. All these tasks demand accurate determination of L_w in the field, and it is not surprising to see more than five decades of acquisition of L_w and continued improvement in instrumentation and data-processing methods. But the long-standing goal of achieving better than 5% accuracy of L_w [33] is hardly achieved [13,30]. This is due to the following: (1) L_w is not a stable property in the field because of rough sea surface [34], unless the environmental condition is perfect (flat surface, clear sky, and stable water property); and (2) the conventional approaches do not obtain a direct measurement of L_w. Hooker and Maritorena [16] presented within 5% consistency of $L_u(0-)$ between in-water deployments, but were limited to measurements of oceanic waters, at local noon, and in the 412–555 nm spectral range. When comparing measurements between in-water and above-water strategies, Zibordi *et al.* [29] indicated that the difference is ~10% for 440 and 550 nm and more than 20% for 670 nm, and the difference reduced to ~5% for the 412–555 nm range for clearer waters [18]. Also note that these results provide a measure of consistency for two datasets, not necessarily the precision of each individual L_w spectrum.

Unlike laboratory measurements where almost all aspects of an experiment can be precisely controlled, field measurements of L_w are inherently subject to various disturbances that are out of the control of an operator. These aspects include rough sea surface, randomly distributed and moving clouds, a stratified upper water column, and wave-induced light focusing, just to name a few. As a result, even if all relevant components could be measured precisely, the spectral L_w determined via methods listed in Table 1 still contains various degrees of uncertainties, and the ground "truth" of L_w is elusive. Specifically, for L_w determined via S1, it is unavoidable that surface-reflected light will be introduced into the measured signal, which has to be removed properly before L_w can be determined [35]. Mobley [17] introduced a simple formula along with a spectrally flat surface-reflectance value (varying with wind speed and viewing angle though). This is more appropriate for overcast sky conditions [13], where the light quality from various angles is nearly the same (i.e., the spectral shape from different directions can be considered identical with negligible error), but could be troublesome for clear-sky days [19,20], where the light from overhead is quite bluer than the light from the horizon. To mitigate this limitation, Zibordi *et al.* [18] suggested to aggressively filter out large values and focus on the lower 20% of data measured from an above-surface platform. By using a slightly different formula for this correction [14,31], Lee *et al.* [19,36] used a more sophisticated processing method to remove the contaminations. In this process, the correction involves two terms: one uses the product of Fresnel reflectance and the reciprocally measured skylight to remove the primary portion of the surface contribution; the other uses a bias to account for the residual contribution and is derived iteratively through optical modeling. Nevertheless, these procedures cannot completely remove surface-reflected light, as the contribution is highly dependent on surface texture, sky-light distribution, as well as the instrument's integration time, and the former two aspects are out of our control.

A significant advantage of S2 is that not only can $L_u(0-)$ be calculated from the vertical profiles of $L_u(z)$ and $E_d(z)$, but also the vertical distribution of absorption and backscattering coefficients [37]. For the purpose of determining L_w, however, this scheme runs into difficulty if the upper water column is stratified, or the water is extremely turbid, or the bottom is quite shallow and/or with seagrass/kelp, situations that make it difficult to extrapolate measurements at a depth to below the surface. In addition, L_u in the longer wavelengths at deeper depths may include more relative contributions from inelastic scattering [38,39], and thus contributes more uncertainties to the determination of $L_u(0-)$. Furthermore, the calculated $L_u(0-)$ has to be subjectively propagated through the interface to get L_w, a step that will introduce some uncertainties.

S3 is a plausible approach for determination of L_w in the field [40,41], as it can effectively avoid difficulties introduced by surface-reflected light and difficulties in obtaining the accurate vertical profiles required by S2. However, no matter how close the sensor is to the surface, the measured signal is not L_w, but $L_u(z)$, which has to be propagated via models through the air–water interface for determination of L_w. Uncertainties will be introduced in this calculation process.

The scheme to directly measure L_w via SBA, although might not be optimized at this point, clearly shows great promise and advantages for accurately measuring L_w in the field. In particular, it significantly reduces the requirement of post-measurement processing, thus making the data product "measured," instead of "calculated." It avoids surface-reflected light through a mechanical design, measures L_w propagating through the interface naturally, and is not limited for environments that are either stratified or with a shallow bottom. Measurement via SBA offers an opportunity to get the ground "truth" of L_w in the field, a goal hardly achieved so far.

The most likely source of uncertainty in the field measurement via SBA comes from two situations: (1) the sensor is submerged into water, and (2) the entire cone rises above the surface. Our results indicate that these contaminations can be quite effectively removed, as both situations would measure significantly higher values [see Eqs. (1) and (2)]. In our data processing here we removed less than 3% of the measured spectra, kept ~97% of the lower values, and achieved ~5% precision. Much higher precision is thus expected if we filter out data more aggressively (say 40%), but an objective decision on

this criterion requires more modeling studies as well as experience with field data. This is also because L_w in the field is inherently not a constant value even in a short time scale. Because of wave-introduced roughness, L_w measured at different times could be slightly different due to wave focusing or variation in the observation angle [42,43]. This variation is highlighted in Fig. 11, where the CV spectrum of the SBA-measured L_w is separated into two groups: one CV spectrum for data collected under prime condition, i.e., when the water surface was calm (wave height <2′) while the sky is clear; and another CV spectrum for conditions not prime. As expected, the CV of SBA-measured L_w under prime condition is systematically smaller (in a range of 2%–5% for the 370–650 nm band) than that under nonprime condition. However, even for the SBA-measured L_w obtained under tough situations, the overall uncertainty is still in a range of 5%–10% for the 370–650 nm band, and that is under the current data-processing scheme (e.g., no screening of clouds). We expect this precision to improve after we carry out more experiments and gain more experience and understanding of the measurement scheme.

The major challenge in accurately measuring L_w via SBA is to minimize the self-shading introduced by the cone as well as by the floating structure, although such shading could be modeled to some degree based on radiative transfer [25,26,44]. Note that self-shading of SBA is positively related to the size of the cone. Minimizing self-shading thus requires a small field of view and a small aperture for the radiometer, as these two factors dictate the size of the cone. It will also require a small floating collar and a longer arm between the sensor and the collar, in order to reduce the intrusion of the system into the light field to be measured by the radiometer.

The scheme of measuring L_w via the SBA also opens the door to taking cost-effective long-term measurement of L_w right on the surface, which is important in obtaining a large volume of data either for calibration/validation of satellite systems or for the study of biogeochemistry. A serious challenge

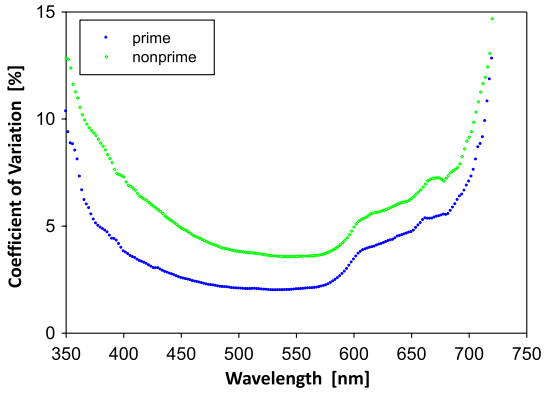

Fig. 11. (Color online) Averaged CV spectrum of SBA-measured L_w; the blue curve is for data under prime measurement conditions and the green curve is for data under nonprime conditions. Prime condition is defined here as calm surface (<2′ wave) and clear sky.

in long-term field deployment in a marine environment is bio-fouling. One strategy to avoid bio-fouling is to establish the AERONET-OC network [35,45], where all sensors are above the surface. But L_w through this system is determined via S1, where some contaminations due to surface-reflected light will not be avoidable [13,17,18]. With the SBA strategy, the sensor will remain in the air, and the bio-fouling will likely happen on the surface of the cone, which might effectively reduce the impact of bio-fouling on the sensor and then on data quality. But this requires dedicated effort to study and characterize the effects and to optimize the design and setup. When a mature and successful setup is available, it could significantly improve the quality and volume of L_w by taking measurements right on the surface. In addition, it could improve the earlier generation of optical drifters [46] for continuous monitoring of water masses at low cost.

7. Conclusions

It is critical to achieve precise and accurate measurement of water-leaving radiance (or remote-sensing reflectance) in the field, and numerous advances in technology have been achieved in recent decades for this goal. The SBA shown here measures water-leaving radiance directly, and achieves high-precision results in the field. This SBA is easily deployable not only in oceanic waters, but also in challenging environments such as shallow waters. Measurement via SBA provides the closest results to the ground truth of water-leaving radiance, and this will certainly aid in achieving the goal of measuring L_w in the field within 5% uncertainty under normal measurement conditions. The results shown here, however, are limited to a few water types and mild sea states. Extensive tests and experiments with SBA in various aquatic environments and sea states in the coming years will not only help the maturation of this measurement approach, but will also provide significant help in the advancement of hydro-optics and ocean (water) color remote sensing.

We thank Wesly Goode of the Naval Research Lab for helping set up the SBA system, Christopher Strait, Mike Twardowski, and Colleen Mouw for helping the field experiment, and Captain Richard C. Pagel of the R/V Gaylord Nelson for professional assistance. Financial support from NASA (Ocean Biology and Biogeochemistry, Energy and Water Cycle, and Applied Sciences programs) and the JPSS VIIRS Ocean Color Cal/Val Project is greatly appreciated. Comments and suggestions from two anonymous reviewers greatly improved this manuscript. This is contribution 309 of the Upstate Freshwater Institute.

References

1. IOCCG, "Remote sensing of ocean colour in coastal, and other optically-complex, waters," in Reports of the International Ocean-Colour Coordinating Group, No. 3, S. Sathyendranath, ed. (IOCCG, 2000).
2. IOCCG, "Remote sensing of inherent optical properties: fundamentals, tests of algorithms, and applications," in Reports

of the International Ocean-Colour Coordinating Group, No. 5, Z.-P. Lee, ed. (IOCCG, 2006), p. 126.
3. H. Gordon, "In-orbit calibration strategy for ocean color sensors," Remote Sens. Environ. **63**, 265–278 (1998).
4. D. K. Clark, M. A. Yarbrough, M. Feinholz, S. Flora, W. Broenkow, Y. S. Kim, B. C. Johnson, S. W. Brown, M. Yuen, and J. L. Mueller, "MOBY, a radiometric buoy for performance monitoring and vicarious calibration of satellite ocean color sensors: measurement and data analysis protocols," NASA Tech. Memo. 2004-211621 (NASA, 2003).
5. K. J. Voss, S. McLean, M. Lewis, C. Johnson, S. Flora, M. Feinholz, M. Yarbrough, C. Trees, M. Twardowski, and D. Clark, "An example crossover experiment for testing new vicarious calibration techniques for satellite ocean color radiometry," J. Atmos. Ocean. Technol. **27**, 1747–1759 (2010).
6. P. J. Werdell, S. W. Bailey, B. A. Franz, A. Morel, and C. R. McClain, "On-orbit vicarious calibration of ocean color sensors using an ocean surface reflectance model," Appl. Opt. **46**, 5649–5666 (2007).
7. G. Zibordi, J.-F. Berthon, F. Mélin, D. D'Alimonte, and S. Kaitala, "Validation of satellite ocean color primary products at optically complex coastal sites: Northern Adriatic Sea, Northern Baltic Proper and Gulf of Finland," Remote Sens. Environ. **113**, 2574–2591 (2009).
8. C. R. McClain, W. E. Esaias, W. Barnes, B. Guenther, D. Endres, S. B. Hooker, G. Mitchell, and R. Barnes, "Calibration and validation plan for SeaWiFS," NASA Tech. Memo. 104566, Vol. **3**, S. B. Hooker and E. R. Firestone, eds. (NASA, 1992), p. 41.
9. H. R. Gordon, "Removal of atmospheric effects from satellite imagery of the oceans," Appl. Opt. **17**, 1631–1636 (1978).
10. H. R. Gordon and M. Wang, "Retrieval of water-leaving radiance and aerosol optical thickness over oceans with SeaWiFS: a preliminary algorithm," Appl. Opt. **33**, 443–452 (1994).
11. M. Wang, "Remote sensing of the ocean contributions from ultraviolet to near-infrared using the shortwave infrared bands: simulations," Appl. Opt. **46**, 1535–1547 (2007).
12. K. G. Ruddick, F. Ovidio, and M. Rijkeboer, "Atmospheric correction of SeaWiFS imagery for turbid coastal and inland waters," Appl. Opt. **39**, 897–912 (2000).
13. D. A. Toole, D. A. Siegel, D. W. Menzies, M. J. Neumann, and R. C. Smith, "Remote-sensing reflectance determinations in the coastal ocean environment: impact of instrumental characteristics and environmental variability," Appl. Opt. **39**, 456–469 (2000).
14. J. L. Mueller, C. Davis, R. Arnone, R. Frouin, K. L. Carder, Z. P. Lee, R. G. Steward, S. Hooker, C. D. Mobley, and S. McLean, "Above-water radiance and remote sensing reflectance measurement and analysis protocols," in *Ocean Optics Protocols for Satellite Ocean Color Sensor Validation, Revision 3, NASA/TM-2002-210004*, J. L. Mueller and G. S. Fargion, eds. (NASA, 2002), pp. 171–182.
15. J. L. Mueller, G. S. Fargion, and C. R. McClain, *Ocean Optics Protocols For Satellite Ocean Color Sensor Validation, Revision 4* (NASA, 2003).
16. S. B. Hooker and S. Maritorena, "An evaluation of oceanographic radiometers and deployment methodologies," J. Atmos. Ocean. Technol. **17**, 811–830 (2000).
17. C. D. Mobley, "Estimation of the remote-sensing reflectance from above-surface measurements," Appl. Opt. **38**, 7442–7455 (1999).
18. G. Zibordi, F. Mélin, S. B. Hooker, D. D'Alimonte, and B. Holben, "An autonomous above-water system for the validation of ocean color radiance data," IEEE Trans. Geosci. Remote Sens. **42**, 401–415 (2004).
19. Z.-P. Lee, Y.-H. Ahn, C. Mobley, and R. Arnone, "Removal of surface-reflected light for the measurement of remote-sensing reflectance from an above-surface platform," Opt. Express **18**, 26313–26342 (2010).
20. D. Doxaran, R. C. N. Cherukuru, and S. J. Lavender, "Estimation of surface reflection effects on upwelling radiance field measurements in turbid waters," J. Opt. Pure Appl. Opt. **6**, 690–697 (2004).
21. R. C. Smith, C. R. Booth, and J. L. Star, "Oceanographic bio-optical profiling system," Appl. Opt. **23**, 2791–2797 (1984).
22. G. Zibordi, D. D'Alimonte, and J. F. Berthon, "An evaluation of depth resolution requirements for optical profiling in coastal waters," J. Atmos. Ocean. Technol. **21**, 1059–1073 (2004).
23. C. D. Mobley, *Light and Water: Radiative Transfer in Natural Waters* (Academic, 1994).
24. Y.-H. Ahn, "Development of redtide & water turbidity algorithms using ocean color satellite," 1999, KORDI Seoul, Korea, p. 287.
25. H. R. Gordon and K. Ding, "Self-shading of in-water optical instruments," Limnol. Oceanog **37**, 491–500 (1992).
26. R. A. Leathers, T. V. Downes, and C. D. Mobley, "Self-shading correction for upwelling sea-surface radiance measurements made with buoyed instruments," Opt. Express **8**, 561–570 (2001).
27. R. W. Austin, "Inherent spectral radiance signatures of the ocean surface," in *Ocean Color Analysis*, S. W. Duntley, ed. (Scripps Institution of Oceanography, 1974). pp. 1–20.
28. H. R. Gordon and D. K. Clark, "Clear water radiances for atmospheric correction of coastal zone color scanner imagery," Appl. Opt. **20**, 4175–4180 (1981).
29. G. Zibordi, S. B. Hooker, J. F. Berthon, and D. D'Alimonte, "Autonomous above-water radiance measurements from an offshore platform: a field assessment experiment," J. Atmos. Ocean. Technol. **19**, 808–819 (2002).
30. S. B. Hooker, G. Lazin, G. Zibordi, and S. D. McLean, "An evaluation of above- and in-water methods for determining water-leaving radiances," J. Atmos. Ocean. Technol. **19**, 486–515 (2002).
31. K. L. Carder and R. G. Steward, "A remote-sensing reflectance model of a red tide dinoflagellate off West Florida," Limnol. Oceanog. **30**, 286–298 (1985).
32. D. Doxaran, N. C. Cherukuru, S. J. Lavender, and G. F. Moore, "Use of a Spectralon panel to measure the downwelling irradiance signal: case studies and recommendations," Appl. Opt. **43**, 5981–5986 (2004).
33. S. Hooker and W. E. Esaias, "An overview of the SeaWiFS project," Eos **74**, 241–246 (1993).
34. J. R. V. Zaneveld, E. Boss, and P. A. Hwang, "The influence of coherent waves on the remotely sensed reflectance," Opt. Express **9**, 260–266 (2001).
35. G. Zibordi, B. Holben, I. Slutsker, D. Giles, D. D'Alimonte, F. Melin, J.-F. Berthon, D. Vandemark, H. Feng, G. Schuster, B. E. Fabbri, S. Kaitala, and J. Seppala, "AERONET-OC: a network for the validation of ocean color primary products," J. Atmos. Ocean. Technol. **26**, 1634–1651 (2009).
36. Z. P. Lee, K. L. Carder, T. G. Peacock, C. O. Davis, and J. L. Mueller, "Method to derive ocean absorption coefficients from remote-sensing reflectance," Appl. Opt. **35**, 453–462 (1996).
37. H. R. Gordon, M. R. Lewis, S. D. McLean, M. S. Twardowski, S. A. Freeman, K. J. Voss, and G. C. Boynton, "Spectra of particulate backscattering in natural waters," Opt. Express **17**, 16192–16208 (2009).
38. A. Morel and B. Gentili, "Radiation transport within oceanic (case 1) water," J. Geophys. Res. **109**, C06008 (2004).
39. B. R. Marshall and R. C. Smith, "Raman scattering and in-water ocean properties," Appl. Opt. **29**, 71–84 (1990).
40. K. J. Voss and A. L. Chapin, "Upwelling radiance distribution camera system, NURADS," Opt. Express **13**, 4250–4262 (2005).
41. K. J. Voss and N. Souaidia, "POLRADS: polarization radiance distribution measurement system," Opt. Express **18**, 19672–19680 (2010).
42. J. R. V. Zaneveld, E. Boss, and A. Barnard, "Influence of surface waves on measured and modeled irradiance profiles," Appl. Opt. **40**, 1442–1449 (2001).
43. A. Morel and B. Gentili, "Diffuse reflectance of oceanic waters (2): bi-directional aspects," Appl. Opt. **32**, 6864–6879 (1993).
44. J. P. Doyle and G. Zibordi, "Optical propagation within a three-dimensional shadowed atmosphere-ocean field: application to large deployment structures," Appl. Opt. **41**, 4283–4306 (2002).
45. G. Zibordi, B. Holben, S. B. Hooker, F. Mélin, J.-F. Berthon, and I. Slutsker, "A network for standardized ocean color validation measurements," Eos **87**, 297 (2006).
46. M. R. Abbott and R. M. Letelier, "Decorrelation scales of chlorophyll as observed from bio-optical drifters in the California Current," Deep-Sea Res. **45**, 1639–1667 (1998).